ARTICLE

Nanocomposites of Carbon Nanotube Fibers Prepared by Polymer Crystallization

Shanju Zhang,[†,‡] Wei Lin,[§] Ching-Ping Wong,[§] David G. Bucknall,[*,†] and Satish Kumar[*,†]

School of Polymer, Textile and Fiber Engineering, Georgia Institute of Technology, Atlanta, Georgia 30332-0295, and School of Materials Sciences and Engineering, Georgia Institute of Technology, Atlanta, Georgia 30332-0245

ABSTRACT Nanocomposites of carbon nanotube fibers have been prepared using controlled polymer crystallization confined in nanotube aerogel fibers. The polyethylene nanocomposites have been investigated by means of polarized optical microscopy (POM), scanning electron microscopy (SEM) and wide-angle X-ray diffraction (WAXD). The individual nanotubes are periodically decorated with polyethylene nanocrystals, forming aligned hybrid shish-kebab nanostructures. After melting and recrystallization, transcrystalline lamellae connecting the adjacent aligned nanotubes develop. Microstructural analysis shows that the nanotubes can nucleate the growth of both orthorhombic and monoclinic crystals of polyethylene in the quiescent state. The tensile strength, modulus, and axial electrical conductivity of these polyethylene/CNT composite fibers are as high as 600 MPa, 60 GPa, and 5000 S/m, respectively.

KEYWORDS: nanocomposites • carbon nanotubes • fibers • polymer crystallization • interface

INTRODUCTION

Carbon nanotube (CNT) fibers have great potential for various applications, not only for the development of high performance lightweight fibers (1−6) but also as the building block of advanced composite materials (7−11). Infiltrating polymer solution into CNT fibers can lead to CNT fiber based nanocomposites. As CNTs in the fibers are aligned and can be millimeters long, the resultant nanocomposites resemble the ideal reinforcing structure of aligned, continuous CNTs in the polymer matrix (11). It has been reported (11) that the epoxy-infiltrated CNT fibers (CNT loading is 40 ± 10 vol %) have a tensile strength of 0.9−1.6 GPa and a modulus of 30−50 GPa, whereas the PVA-infiltrated CNT fibers exhibit tensile strength and modulus of 0.7−1.3 and 20−35 GPa, respectively.

In semicrystalline polymer nanocomposites, CNTs also act as an orientation template and nucleating agent for polymer crystallization (12−17). At CNT surfaces, the polymer forms an ordered crystal layer with molecular chains orienting along the CNT axis. The ordered polymer packing on the CNT can enhance load transfer from the polymer matrix to the CNTs across the interface and thereafter improve the mechanical properties of the nanocomposites (18−20). Recently, we have reported polymer transcrystalline structures induced by CNTs during isothermal melting crystallization of polypropylene (20). It has been found that the tensile strength and modulus of transcrystallized polypropylene with 3 wt % CNTs are 200% higher than those of the pure polypropylene crystallized by itself. It has been suggested that the effective load transfer from the transcrystallized polypropylene layer to CNTs contribute to such an improvement (20).

In this work, we report CNT fiber-based nanocomposites prepared by controlled polymer crystallization from both solution and melt. Both hybrid shish-kebab nanostructures and transcrystalline lamellae around the individual nanotubes are discovered and the mechanical properties of resultant nanocomposites are evaluated.

EXPERIMENTAL SECTION

Vertically aligned CNT arrays were synthesized by chemical vapor deposition (CVD) (21−23). The resultant CNTs were multiwalled with an average 10 nm diameter and 1.0 mm length. The CNT fibers were produced from the aligned CNT arrays using a dry-drawing process (24). The intertube spacing in the CNT fibers was in the order of 10−100 nm. The as-drawn CNT aerogel fibers were immersed in 0.01 wt % solution of high-density polyethylene (HDPE, MFI = 12 g/10 min under 190 °C/2.16 kg, Aldrich Co.) or ultrahigh molecular weight polyethylene (UHMWPE, average M_w = 3−6 × 10^6 g/mol, Aldrich Co.) in *p*-xylene at 120 °C for 10 min. The system temperature was then reduced to 103 ± 1 °C and annealed for varying lengths of time between 2 and 12 h. The fibers were then washed in ethanol and dried at 50 °C under a vacuum overnight. The isothermal melting crystallization of the resultant composite fibers was conducted in an oven, where the specimens were annealed at 180 °C for 5 min and then at 120 °C overnight.

The cross-sections of the composite fibers were obtained by the microtoming samples that had been prepared by immersing in a resin mixture of methyl methacrylate (75 mL), dibutyl phthalate (5 mL), and benzoyl peroxide (2.5 g). The mixture was subsequently cured at 37 °C under a vacuum overnight (24). The composite fibers embedded in the polymer resin were then microtomed by a diamond knife. After coating with gold the specimens were examined in a scanning electron microscopy (SEM, LEO 1530) operated at 5 kV. Optical microscopy was conducted on a Leica DMRX optical microscope with cross polars. Thermogravimetric analysis (TGA) was performed using

* Corresponding author. E-mail: david.bucknall@ptfe.gatech.edu (D.B.); satish.kumar@ptfe.gatech.edu (S.K.).

Received for review February 27, 2010 and accepted May 19, 2010

† School of Polymer, Textile and Fiber Engineering, Georgia Institute of Technology.

‡ Current address: Department of Chemical Engineering, Yale University, New Haven, CT 06511.

§ School of Materials Sciences and Engineering, Georgia Institute of Technology.

DOI: 10.1021/am1001663

Published on Web 05/27/2010

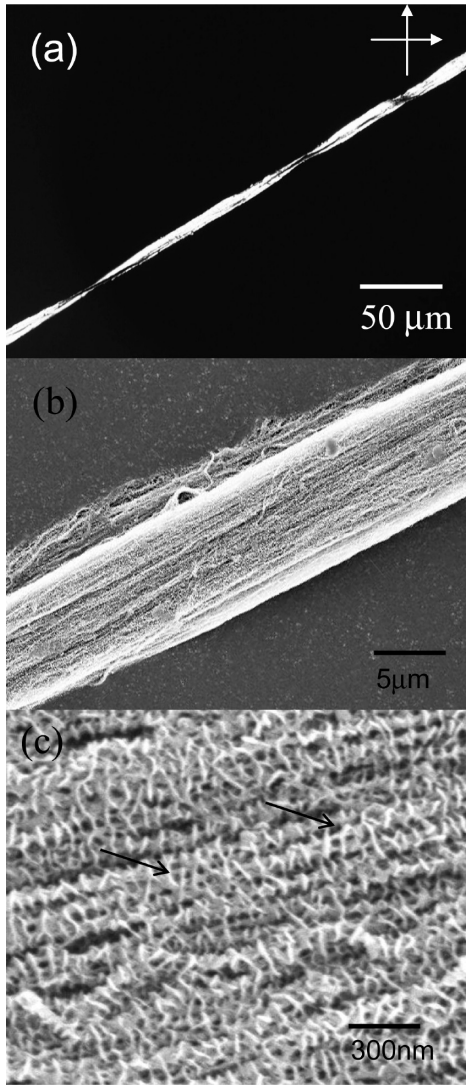

FIGURE 1. HDPE nanocomposite fiber by solution crystallization for 2 h. (a) Optical image under cross polars. Polarizer and analyzer directions are shown by arrows, (b) SEM image at low-magnification, (c) SEM image at high-magnification. Arrows in c show polymer nanocrystals grown on adjacent nanotubes.

a TGA-Q5000 (TA Instruments) with a heating rate of 10 °C/min under nitrogen. Wide-angle X-ray diffraction (WAXD) patterns were obtained in transmission mode using a Rigaku Micromax-002 (λ = 0.15418 nm) and Rigaku R-axis IV ++ detection system. The mechanical properties of the composite fibers were determined using RSA III solids analyzer (Rheometric Scientific, Co.) at room temperature at a test speed of 0.05 mm/min with a gauge length of 10 mm.

RESULTS AND DISCUSSION

Figure 1a shows a typical optical image under cross polars of the CNT-HDPE nanocomposite fiber after 2 h solution crystallization. The nanocomposite fiber is highly birefringent. The SEM image of the nanocomposite fiber shows periodic, disk-shaped PE nanocrystals, leading to aligned hybrid shish-kebab nanostructures (Figure 1b and c). CNT-induced hybrid shish-kebab nanostructures in the quiescent state were initially reported by Li et al. in the mixture of CNTs and HDPE during controlled solution crystallization (25). CNT-induced hybrid shish-kebab nanostructures have now been reported in polymers of nylon (26), poly(vinyl alcohol) (PVA) (27), and polyethylene-*b*-poly(ethylene oxide) (PE-*b*-PEO) (16) using the similar mixing methods. In contrary, PE nanocrystals in this work grow inside the aligned CNT fibers. Therefore, PE nanocrystals not only form on the individual CNT surface but also develop on across a number of CNTs (Figure 1c, see arrows). This observation is different from the classical shish-kebab structures where the kebabs only wrap on one shish (28−30).

Figure 2 shows SEM images of HDPE and UHMWPE nanocomposites prepared by controlled solution crystallization for varying amounts of time. As expected, aligned hybrid shish-kebab nanostructures are observed in both systems. After 2 h of crystallization, in both HDPE and UHMWPE samples, nanocrystals were observed on the CNT surfaces (Figure 2a,c). Average lateral dimensions and periodicity of spacing between the nanocrystals of ∼30 ± 15 nm and ∼40 ± 20 nm, respectively, were observed in both the HDPE and UHMWPE matrices. The CNT loading in the nanocomposites annealed for short solution crystallization times calculated be ∼70 wt % by TGA. Increasing crystallization time to 12 h resulted in extensive PE nanocrystal growth on the CNTs (Figure 2b,d). PE nanocrystals have grown to such an extent that the individual CNTs are difficult to be identified. CNT loading in the 12 h crystallized composite fibers was ∼30 wt %.

PE nanocrystals have been observed to grow on more than one adjacent CNTs. This leads to an interlocking of two or more CNTs by a polyethylene crystal. It is conceivable that this unique morphology enhances the load transfer between polyethylene nanocrystals and CNTs, when the sample is stretched (31).

WAXD data of HDPE and UHMWPE nanocomposites after 2 and 12 h of crystallization are shown in Figure 3. With increasing crystallization time from 2 to 12 h, the degree of crystalllinity increased from 25−30% to 60−65%, respectively. The high level of crystallinity is attributed to more complete PE crystallization in dilute solution. All the samples show similar diffraction patterns. The 2D WAXD patterns are anisotropic with the most intensity at the equator associated with the oriented PE nanocrystals and CNTs. This observation is consistent with the optical results (Figure 1a). The reflection at $2\theta = 25.5°$ comes from the graphite (002) plane of the CNTs. The main peaks at $2\theta = 21.5$ and 23.9° are indexed as (110) and (200) planes of the orthorhombic form of PE, respectively (32). An additional reflection located at $2\theta = 19.5°$ is indexed as the (010) plane of the monoclinic form of PE (32). In general, the monoclinic form of PE is metastable in pure polymers and is only obtained under either high pressure (33) or large deformations, for example, during mechanical stretching (34). The formation of monoclinic PE crystals during quiescent crystallization at atmosphere pressure, observed in the current work, demonstrates that the CNTs act as a nucleating agent for the monoclinic PE crystallization.

To study the effect of thermal treatments on the polymer morphology in the nanocomposites, the effect of isothermal

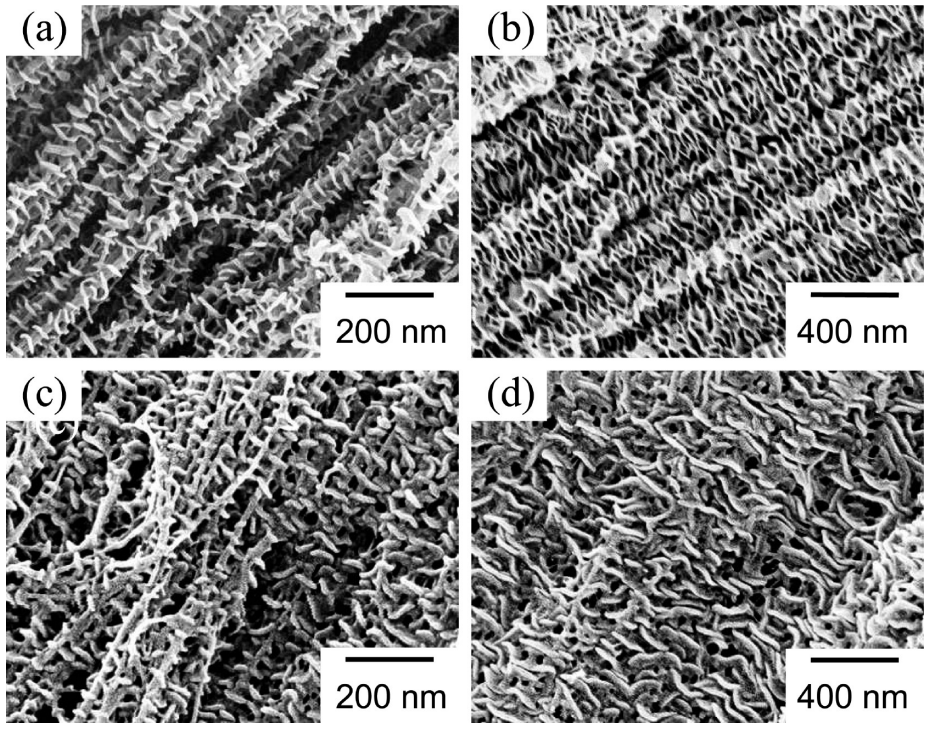

FIGURE 2. SEM images of nanocomposite fibers by solution crystallization. HDPE composites with (a) 2 and (b) 12 h of crystallization, UHMWPE composites with (c) 2 and (d) 12 h of crystallization.

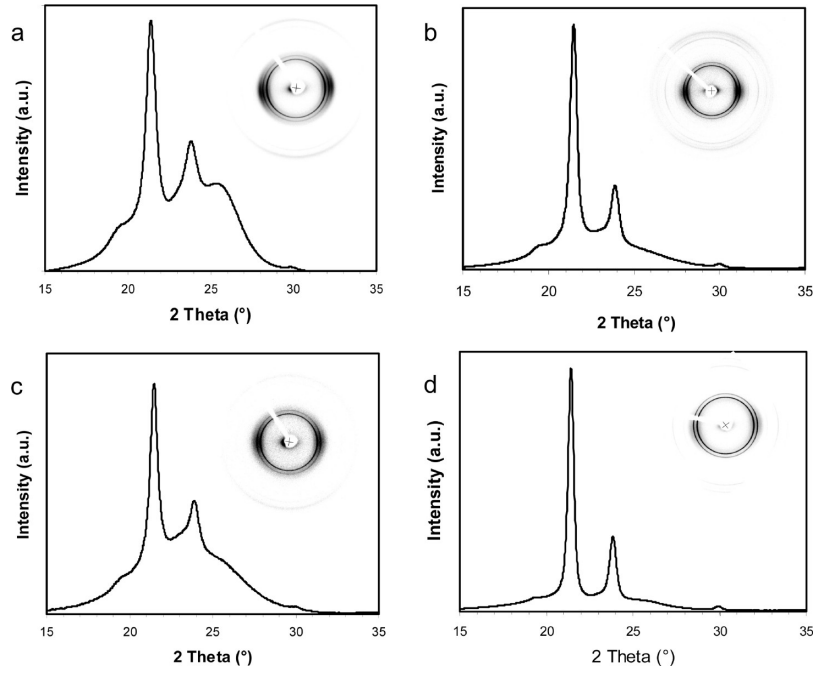

FIGURE 3. WAXD data of nanocomposite fibers by solution crystallization. HDPE composites with (a) 2 and (b) 12 h of crystallization, UHMWPE composites with (c) 2 and (d) 12 h of crystallization. The insets show 2D WAXD patterns.

melting recrystallization was investigated. Figure 4a shows a typical SEM image of a melt recrystallized nanocomposite containing 30 wt % CNT. The aligned hybrid shish-kebab nanostructures formed after solution crystallization are replaced by oriented crystalline lamellae connecting the adjacent aligned CNTs. This supramolecular hybrid nanostructure is identified as the transcrystalline interphase with polymer chains parallel to the CNT axis (15, 17, 20). WAXD patterns of melting recrystallized nanocomposites are similar to those of solution crystallized nanocomposites (Figure 4b). PE orientation along the CNT axis is apparent and both orthorhombic and monoclinic forms of PE are identified.

The cross-sectional areas of the nanocomposite fibers used to calculate their mechanical properties were measured from SEM images (Figure 5). Panels a and b in Figure 6 show typical stress–strain curves of the HDPE and UHMWPE

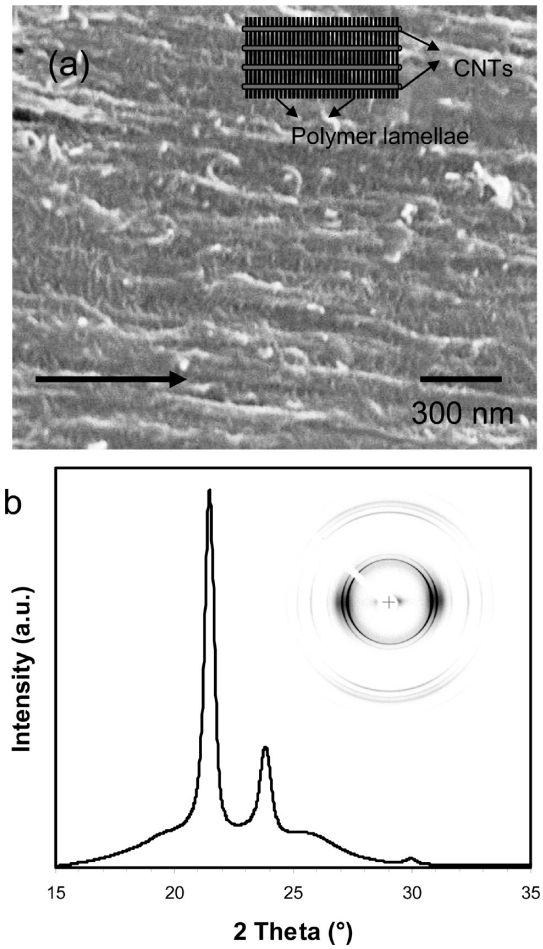

FIGURE 4. HDPE nanocomposite fibers with 30 wt % CNTs after melting and recrystallization. (a) SEM image and (b) WAXD data. The inset of a shows schematic illustration of transcrystalline nanostructures and the inset of b shows the 2D WAXD pattern. The arrow in a shows the fiber axis.

nanocomposites, respectively, with characteristic data from these measurements are listed in Table 1. As a comparison, the data for pure CNT fibers after densification in ethanol are also included. The pure CNT fibers are weak because of the slippage of CNTs during stretching (24). With PE nanocrystals as a binder, the nanocomposites showed improved mechanical properties as expected. With hybrid shish-kebab nanostructures, both HDPE and UHMWPE nanocomposites showed ~70−300% increase in Young's modulus depending on the CNT loading. UHMWPE nanocomposites of CNT fibers with 70 wt % CNTs show modulus values as high as ~60 GPa. It should be noted that the cross-sectional areas used for calculating the mechanical properties might be slightly overestimated, because the polymer resin used for microtoming could have penetrated into the fiber before curing and thereby swollen the fiber in these SEM samples (9). As a result, the actual mechanical properties of the nanocomposites might be slightly larger than we have determined.

In general, PE shish-kebab structures formed by the chain-folded kebab lamellae typically have a low stiffness of ~0.2 GPa (35). However, in systems where the PE kebabs lamellae are able to form a parallel and interlocking arrangement, the load is able to transfer from PE kebab lamellae to chain-extended shish. As a result, the shish-kebabed PE have moduli values close to those of chain-extended shish (28−30). PE processed by stirring and surface-growth techniques have also shown to develop such interlocking shish-kebab structures evidenced by TEM and the modulus of the resultant PE can reach up to 50−90 GPa (30). It is reasonable to assume that a similar interlocking of hybrid shish-kebab nanostructures observed in this work is responsible for the high moduli values in the nanocomposites.

After melting and recrystallization, ductile deformation behavior is observed for both HDPE and UHMWPE nanocomposites. This observation is attributed to the presence of the transcrystalline interphase, the growth of which is induced by the individual CNTs. The stretching of the melt crystallized nanocomposites was accompanied by the development of necking. Recently, we reported that CNTs induced polypropylene transcrystallinity in the bulk with similar ductile deformation (20). It is assumed that the transcrystalline lamellae are being unfolded during stretching, which contributes to the large elongation and consequently plastic deformation observed in these structures (36). As a result of the transcrystallinity, the HDPE and UHMWPE nanocomposites in this work also possess high tensile strength and modulus. The effective load transfer from the transcrystalline PE to individual CNTs may contribute to such high mechanical performance.

The structure of these nanocomposite fibers also plays a significant role in their electrical conductivity capabilities. The DC electrical conductivity of the nanocomposite fibers

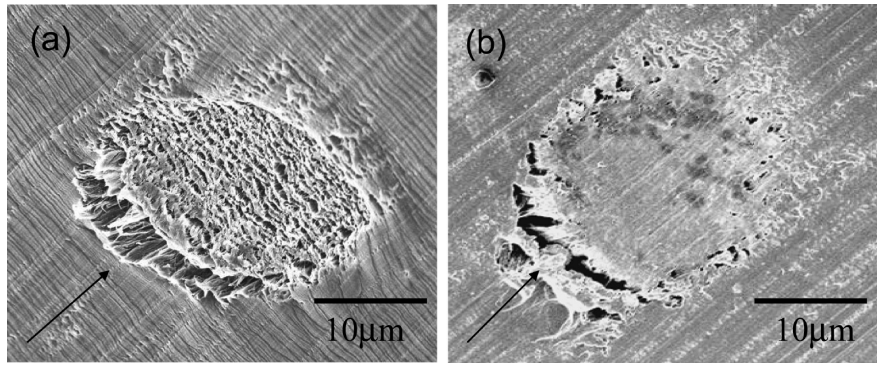

FIGURE 5. SEM images of cross sections of HDPE nanocomposite fibers with (a) 70 and (b) 30 wt % CNTs. Arrows show the cutting directions.

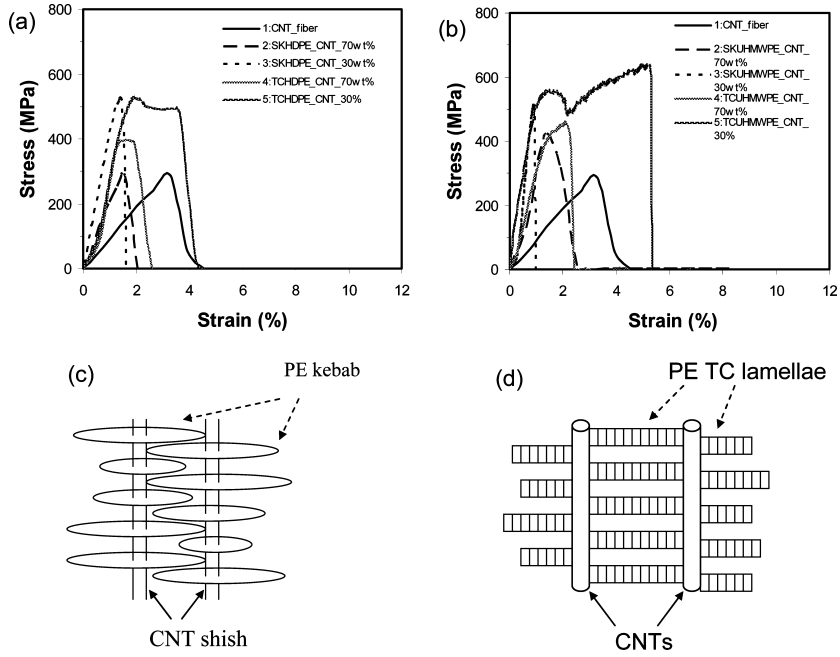

FIGURE 6. Stress–strain curves of (a) HDPE nanocomposites, (b) UHMWHE nanocomposites; schematic illustration of (c) interlocking of hybrid shish-kebab nanostructure and (d) transcrystalline nanostructure.

Table 1. Mechanical Data of CNT-PE Nanocomposites with Shish-Kebab (SK) and Transcrystalline (TC) Structures

samples	CNT loading (wt%)	strength (GPa)	modulus (GPa)	elongation to break (%)
pure CNT fiber	100	0.30 ± 0.05	15 ± 5	3.5 ± 0.5
CNT-HDPE-SK2h	70	0.50 ± 0.18	45 ± 18	1.2 ± 0.2
CNT-HDPE-SK12h	30	0.35 ± 0.10	25 ± 15	2.0 ± 0.6
CNT-HDPE-TC2h	70	0.55 ± 0.22	40 ± 10	3.0 ± 1.0
CNT-HDPE-TC12h	30	0.40 ± 0.24	40 ± 8	2.0 ± 1.2
CNT-UHMWPE-SK2h	70	0.55 ± 0.15	60 ± 15	1.5 ± 0.5
CNT-UHMWPE-SK12h	30	0.40 ± 0.20	35 ± 25	2.2 ± 1.0
CNT-UHMWPE-TC2h	70	0.60 ± 0.25	55 ± 20	4.5 ± 1.5
CNT-UHMWPE-TC12h	30	0.43 ± 0.20	30 ± 18	2.0 ± 1.3

was determined along the fiber axis using a two-point probe test. The current–voltage (I–V) curves of the nanocomposite fibers were linear as shown by a typical set of results in Figure 7. The room temperature axial conductivity for all the samples is in the range of $\sim 5 \pm 1 \times 10^3$ S/m, which as may be anticipated is less than that of the pure CNT fibers ($\sim 5 \times 10^4$ S/m). However, the conductivity of the composite is remarkably high and reflects both the high CNT content as well as the CNTs being continuous and highly aligned.

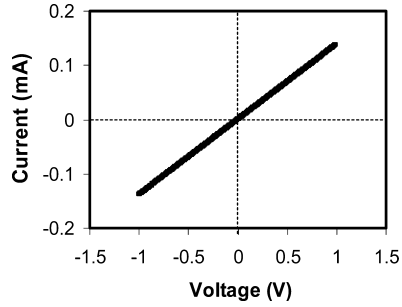

FIGURE 7. Typical current (I)–voltage (V) plot of an HDPE nanocomposite fiber.

CONCLUSIONS

We have studied carbon nanotube fiber-based nanocomposites prepared by controlled polymer crystallization. In a dilute solution, polyethylene diffuses into the nanotube aerogel fibers and crystallizes on the individual nanotube surface in a folded periodic fashion. The resulting polymer nanocrystals form perpendicular to the nanotube axis, forming aligned hybrid shish-kebab nanostructures. After melting recrystallization, the transcrystalline lamellae are produced which bridge between the adjacent aligned nanotubes. Structural analysis showed that nanotubes act as an oriented template and nucleating agent for PE crystallization in both orthorhombic and monoclinic forms. The PE nanocomposites with shish-kebab nanostructures and transcrystalline interphase exhibited high tensile strength and modulus. The effective load transfer from the ordered polymer crystals to the individual CNTs contributes to the good mechanical performance. The present technology provides potential advantages for preparing high-performance nanocomposites with high loading of aligned carbon nanotubes, as polymer crystallization improves the strong physical bonding be-

tween the polymer and nanotubes without damaging the pristine nanotube structures.

Acknowledgment. Financial support from the Air Force Office of Scientific Research and the National Science Foundation are gratefully acknowledged.

REFERENCES AND NOTES

(1) Koziol, K.; Vilatela, J.; Moisala, A.; Motta, M.; Cunniff, P.; Sennett, M.; Windle, A. *Science* **2007**, *318*, 1892.
(2) Zhang, M.; Atkinson, K. R.; Baughman, R. H. *Science* **2004**, *306*, 1358.
(3) Zhang, S. J.; Kumar, S. *Small* **2008**, *4*, 1270.
(4) Zhang, X. F.; Li, Q. W.; Holesinger, T. G.; Arendt, P. N.; Huang, J. Y.; Kirven, P. D.; Clapp, T. G.; DePaula, R. F.; Liao, X. Z.; Zhao, Y. H.; Zheng, L. X.; Peterson, D. E.; Zhu, Y. T. *Adv. Mater.* **2007**, *19*, 4198.
(5) Zhang, S. J.; Koziol, K. K. K.; Kinloch, I. A.; Windle, A. H. *Small* **2008**, *4*, 1217.
(6) Behabtu, N.; Green, M. J.; Pasquali, M. *Nano Today* **2008**, *3*, 24.
(7) Peng, H. S. *J. Am. Chem. Soc.* **2008**, *130*, 42.
(8) Peng, H.; Jain, M.; Peterson, D. E.; Zhu, Y.; Jia, Q. *Small* **2008**, *4*, 1964.
(9) Zhang, S.; Zhu, L.; Wong, C.-P.; Kumar, S. *Macromol. Rapid Commun.* **2009**, *30*, 1936.
(10) Xiao, L.; Liu, P.; Liu, L.; Jiang, K.; Feng, X. F.; Wei, Y.; Qian, L.; Fan, S. S.; Zhang, T. H. *Appl. Phys. Lett.* **2008**, *92*, 3.
(11) Ma, W.; Liu, L.; Zhang, Z.; Yang, R.; Liu, G.; Zhang, T.; An, X.; Yi, X.; Ren, Y.; Niu, Z.; Li, J.; Dong, H.; Zhou, W.; Ajayan, P. M.; Xie, S. *Nano Lett.* **2009**, *9*, 2855.
(12) Minus, M. L.; Chae, H. G.; Kumar, S. *Polymer* **2006**, *47*, 3705.
(13) Zhang, S.; Kumar, S. *Macromol. Rapid Commun.* **2008**, *29*, 557.
(14) Haggenmueller, R.; Fischer, J. E.; Winey, K. I. *Macromolecules* **2006**, *39*, 2964.
(15) Brosse, A. C.; Tence-Girault, S.; Piccione, P. M.; Leibler, L. *Polymer* **2008**, *49*, 4680.
(16) Li, B.; Li, L.; Wang, B.; Li, C. Y. *Nat. Nanotechnol.* **2009**, *4*, 358.
(17) Lu, K. B.; Grossiord, N.; Koning, C. E.; Miltner, H. E.; van Mele, B.; Loos, J. *Macromolecules* **2008**, *41*, 8081.
(18) Coleman, J. N.; Cadek, M.; Ryan, K. P.; Fonseca, A.; Nagy, J. B.; Blau, W. J.; Ferreira, M. S. *Polymer* **2006**, *47*, 8556.
(19) Coleman, J. N.; Cadek, M.; Blake, R.; Nicolosi, V.; Ryan, K. P.; Belton, C.; Fonseca, A.; Nagy, J. B.; Gun'ko, Y. K.; Blau, W. J. *Adv. Funct. Mater.* **2004**, *14*, 791.
(20) Zhang, S.; Minus, M. L.; Zhu, L. B.; Wong, C. P.; Kumar, S. *Polymer* **2008**, *49*, 1356.
(21) Lin, W.; Xiu, Y. G.; Jiang, H. J.; Zhang, R. W.; Hildreth, O.; Moon, K. S.; Wong, C. P. *J. Am. Chem. Soc.* **2008**, *130*, 9636.
(22) Lin, W.; Moon, K. S.; Zhang, S. J.; Dong, Y.; Shang, J. T.; Chen, M. X.; Wong, C. P. *ACS Nano* **2010**, *4*, 1716.
(23) Lin, W.; Moon, K. S.; Wong, C. P. *Adv. Mater.* **2009**, *21*, 2421.
(24) Zhang, S.; Zhu, L.; Minus, M. L.; Chae, H. G.; Jagannathan, S.; Wong, C. P.; Kowalik, J.; Roberson, L. B.; Kumar, S. *J. Mater. Sci.* **2008**, *43*, 4356.
(25) Li, L. Y.; Li, C. Y.; Ni, C. Y. *J. Am. Chem. Soc.* **2006**, *128*, 1692.
(26) Li, L. Y.; Li, C. Y.; Ni, C. Y.; Rong, L. X.; Hsiao, B. *Polymer* **2007**, *48*, 3452.
(27) Zhang, F.; Zhang, H.; Zhang, Z. W.; Chen, Z. M.; Xu, Q. *Macromolecules* **2008**, *41*, 4519.
(28) Smook, J.; Torfs, J. C. M.; Pennings, A. J. *Makromol. Chem., Macromol. Chem. Phys.* **1981**, *182*, 3351.
(29) Bashir, Z.; Odell, J. A.; Keller, A. *J. Mater. Sci.* **1984**, *19*, 3713.
(30) Odell, J. A.; Grubb, D. T.; Keller, A. *Polymer* **1978**, *19*, 617.
(31) Zhang, S.; Lin, W.; Yu, X.; Wong, C.-P.; Cheng, S. Z. D.; Bucknall, D. G. *Macromol. Chem. Phys.* **2010**, *211*, 1003.
(32) Uehara, H.; Nakae, M.; Kanamoto, T.; Ohtsu, O.; Sano, A.; Matsuura, K. *Polymer* **1998**, *39*, 6127.
(33) Fontana, L.; Vinh, D. Q.; Santoro, M.; Scandolo, S.; Gorelli, F. A.; Bini, R.; Hanfland, M. *Phys. Rev. B* **2007**, *75*, 11.
(34) Butler, M. F.; Donald, A. M.; Bras, W.; Mant, G. R.; Derbyshire, G. E.; Ryan, A. J. *Macromolecules* **1995**, *28*, 6383.
(35) Smook, J.; Pennings, A. J. *J. Appl. Polym. Sci.* **1982**, *27*, 2209.
(36) Hata, T.; Ohsaka, K.; Yamada, T.; Nakamae, K.; Shibata, N.; Matsumoto, T. *J. Adhes.* **1994**, *45*, 125.

AM1001663